THE JOURNAL OF PHYSICAL CHEMISTRY B

Article

pubs.acs.org/JPCB

Equilibrium and Dynamical Characteristics of Imidazole Langmuir Monolayers on Graphite Sheets

Javier Rodriguez,[†,‡] M. Dolores Elola,[†] and D. Laria*[,†,§]

[†]Departamento de Física de la Materia Condensada, Comisión Nacional de Energía Atómica, Avenida Libertador 8250, 1429 Buenos Aires, Argentina

[‡]ECyT, UNSAM, Martín de Irigoyen 3100, 1650 San Martín, Provincia de Buenos Aires, Argentina

[§]Departamento de Química Inorgánica Analítica y Química-Física e INQUIMAE, Facultad de Ciencias Exactas y Naturales, Universidad de Buenos Aires, Ciudad Universitaria, Pabellón II, 1428 Buenos Aires, Argentina

ABSTRACT: Using molecular dynamics techniques, we examine structural and dynamical characteristics of liquid-like imidazole (Im) monolayers physisorbed onto a planar graphite sheet, at T = 384 K. Our simulations reveal that molecular orientations in the saturated monolayer exhibit a bistable distribution, characterized by an inner parallel arrangement of the molecules in close contact with the substrate and a slanted alignment, in those lying in adjacent, outer locations. Compared to the results found in three-dimensional, bulk phases, the analysis of the spatial correlations between sites participating in hydrogen bonding shows a clear enhancement of the intermolecular interactions, which also leads to stronger dipolar correlations. As a result, the gross structural features of the monolayer can be cast in terms of mesoscopic domains, comprising units articulated via winding hydrogen bonds, that persist along typical time intervals of a few tens of picoseconds. On the dynamical side, a similar comparison of the characteristic decorrelation time for orientational motions shows a 4-fold increment. Contrasting, the reduction of the system dimensionality leads to a larger diffusion constant. Possible substrate-induced anisotropies in the diffusive motions are also investigated.

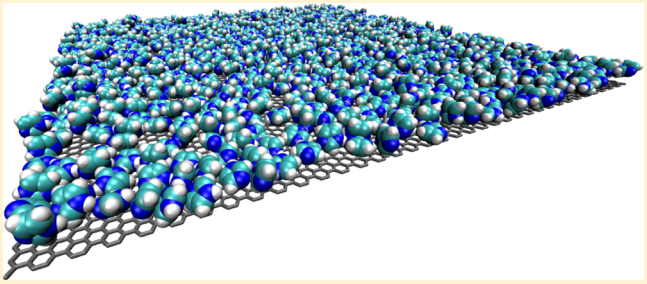

I. INTRODUCTION

Proton transfer in solution represents a key controlling step in a variety of important biological and technological processes.[1,2] In recent years, a large body of experimental and theoretical studies have been conducted to unveil the characteristics of this reactive process in aqueous media.[3−5] From a dynamical perspective, perhaps the most striking feature that characterizes aqueous protons from the rest of simple electrolytes is the possibility of participating in the classical Grotthus shuttling mechanism,[6] operated via a sequence of translocation events along chains of hydrogen-bonded water molecules. Yet, this singular amphiprotic mechanism is not restricted to aqueous environments, and it is also found in several organic solvents, imidazole (Im) and its derivatives being some of the most widely investigated.[7−10] In addition to isotropic fluid phases, new strategies have been recently conceived to enhance proton transport in Im-related compounds by altering the geometrical arrangement of the charge carrier units. For example, Im-based proton exchange membranes have been proposed as alternative components of fuel cells operated at high temperatures.[11−16] In these systems, proton conducting Im moieties are anchored at the surface of mesoporous materials.

The subject of the present work deals with the effects derived from the reduction in dimensionality on structural and dynamical characteristics of liquid-like phases of Im. To that end, we conducted massive molecular dynamics simulations on systems comprising an Im adlayer physisorbed onto a planar graphite sheet. This represents a first step toward the analysis of the transport of excess protons along these monolayers. We remark that the present results provide a microscopic description that complements the one obtained from previous neutron scattering experiments,[17] in which the structure and the diffusion of these adlayers have been examined below and above the corresponding melting point. One intriguing conclusion from the scattering signals in these liquid films would indicate the presence of a strong correlation between details of the underlying surface lattice that, in turn, would result in anisotropic diffusive motions.

In a broader context, the present analysis shares common elements with a large body of previous experimental and simulation studies in which the behaviors of monolayers comprising a variety of organic compounds have been examined.[18−22] At a first glance, and due to the "similarities" in their overall molecular shapes, the adsorption of Im would look akin to that presented by aromatic molecules with similar planar geometries, such as benzene.[23−25] Yet, as we will show,

Special Issue: Branka M. Ladanyi Festschrift

Received: September 3, 2014
Revised: November 11, 2014

   dx.doi.org/10.1021/jp508913w | J. Phys. Chem. B XXXX, XXX, XXX−XXX

differences in the effective intermolecular coupling—most notably, those introduced by hydrogen bonding (HB)—are sufficiently strong so as to induce well differentiated, two-dimensional (2d) arrangements that should be absent in dense benzene monolayers, in which the resulting packing is mainly controlled by excluded volume effects.

The rest of the work is organized as follows: in section II we describe the model and technical procedures. The results of our simulations are presented in section III, whereas, in the last section, we summarize the most important conclusions.

II. MODEL AND SIMULATION PROCEDURES

We performed molecular dynamics (MD) simulations on periodic systems, involving a 2d film composed of N_{Im} = 872 Im molecules, adsorbed on a planar graphite sheet. Imidazole molecules were modeled as fully flexible moieties comprising nine interaction sites (see Figure 1). Intramolecular interactions

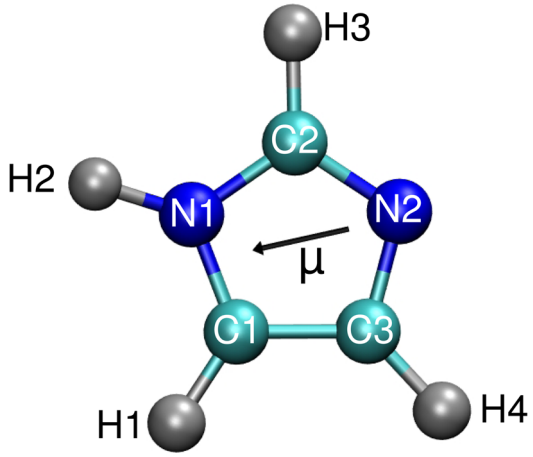

Figure 1. Imidazole. The central arrow indicates the direction of the dipole moment.

included the standard stretching, bending, and dihedral contributions, whereas intermolecular interactions were considered as a sum of pair decomposable site−site contributions, involving dispersion (Lennard-Jones) and Coulomb terms. The potential parameters corresponded to the CHARMM27 force field and are listed in detail in ref 26. With this parametrization, the resulting dipolar moment of the Im is close to 3.9 D and its direction practically coincides with the vector joining atoms N1 and N2. The graphite substrate was modeled as a bilayer composed of 18432 uncharged C atoms, which remained fixed in a hexagonal arrangement at interatomic distances r_{cc} = 1.42 Å, with an interlayer distance of 3.35 Å. The length and energy Lennard-Jones parameters for the C atoms were fixed at σ_c = 3.55 Å and ϵ_c = 0.07 kcal mol^{-1}, respectively. Potential parameters for cross-interactions involving Im-substrate sites were obtained by implementing the standard Lorentz−Berthelot arithmetic and geometric means. Long-range interactions derived from the Coulomb terms of the potential energy were handled by adopting an Ewald sum scheme.[27,28] The dimensions of the simulation box were set to L_x = 153.4 Å, L_y = 157.4 Å, and L_z = 150 Å, which yields an average surface density for the adlayer of $\rho_s = 3.6 \times 10^{-2}$ Å^2. This value agrees with experimental estimates for the saturated monolayer obtained from diffraction experiments.[17] The temperature of the system was fixed at T = 384 K. To gauge the effects of the reduction in the system dimensionality, we also performed simulations of a three-dimensional (3d), isotropic fluid phase, with a global density ρ_{blk} = 0.00911 Å^{-3} at the same temperature, which is ∼50% above the normal melting point of bulk Im. In addition a few test runs were also performed on adsorbed films at T = 250 K, which is ∼5% above the reported melting point of the monolayer.

Average values correspond to, previously thermalized, microcanonical runs lasting typically 10 ns. The thermalization process involved a series of runs in which the temperature of the monolayers was taken up to T = 450 K for about 2 ns; from then on, final temperatures were reached by slowly cooling the systems, along additional ∼1 ns periods. With this procedure, the uncertainties in the statistical averages were kept below 2−3%.

III. RESULTS

A. Structural Characteristics. We will begin our analysis by examining the structural characteristics of the adsorbed monolayer. To that end, it will be instructive to consider a local system of coordinates, oriented such that its z-axis points perpendicularly, away from the graphite foil, with its origin located at the outermost C-layer, in contact with the adsorbed Im film. In the bottom panel of Figure 2 we present profiles for the normalized density of adsorbates at low and high temperatures, namely,

$$\rho_z(z) = \frac{1}{N_{Im}} \sum_{i=1}^{N_{Im}} \langle \delta(Z_i - z) \rangle \tag{1}$$

where Z_i identifies the center of mass of the ith Im moiety. The overall characteristics of the line shapes of the two curves look similar and exhibit main peaks at $z \sim 3.60$ Å. The areas under these peaks, $N(z)$, include roughly half of the total number of molecules. Approximately 1 Å further away from the surface, i.e., at $z \sim 4.60$ Å, one observes secondary peaks, which include contributions from percentages close to ∼40−45% of the total number of molecules; a much more detailed inspection reveals that, at high temperatures, a small fraction close to ∼5% of the adsorbed molecules lies at distances approximately twice as long as the location of the main peak.

The simultaneous analysis of spatial and orientational correlations provides additional information about the previous profiles. In the two top panels of Figure 2, we present contour plots for two-dimensional probability distributions of the following type:

$$P(z, \cos\theta) \propto \sum_{i=1}^{N_{Im}} \langle \delta(Z_i - z)\, \delta(|\cos\theta_i| - \cos\theta) \rangle \tag{2}$$

where $\cos\theta_i$ represents the z-component of the unit vector perpendicular to the molecular plane of the ith imidazole molecule. Clearly, the closest peak at $r \sim 3.60$ Å correlates with adsorbed molecules exhibiting their molecular plane parallel to the interface, whereas the adjacent one includes molecules with slanted orientations. Finally, the outermost profile corresponds to a few stacked molecules lying on top of the previous two layers, which exhibit a much broader spectrum of overall orientations. In passing, we remark that the presence of orientational distributions with bimodal characteristics was found to play an important role as a controlling agent of melting transitions of ethylene-on-graphite monolayers.[29,30]

dx.doi.org/10.1021/jp508913w | J. Phys. Chem. B XXXX, XXX, XXX−XXX

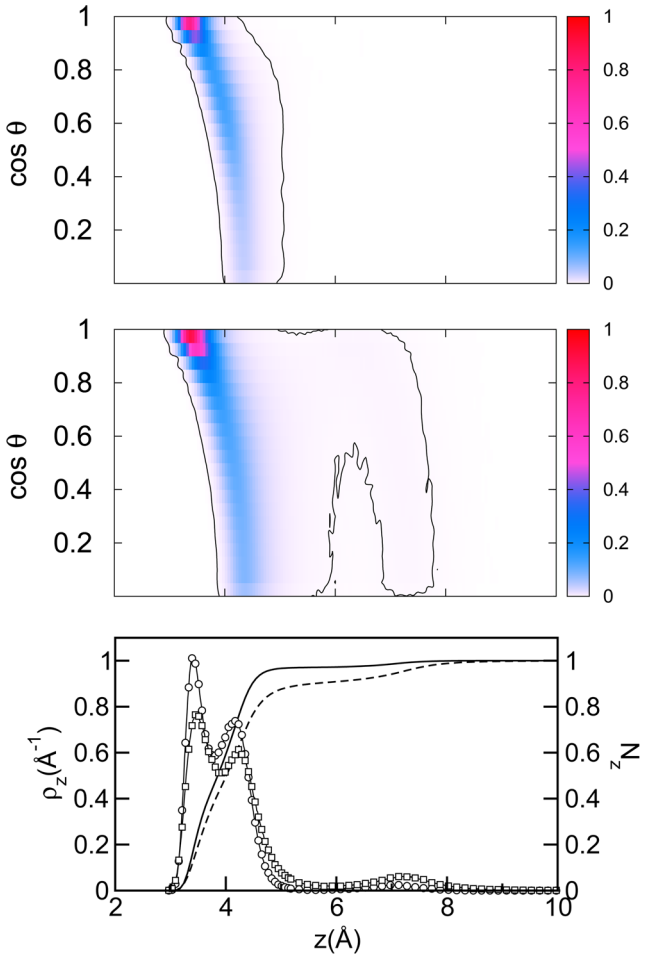

Figure 2. Bottom panel: local density of the adsorbates along perpendicular directions with respect to the interface at different temperatures. Also shown are results for the corresponding cumulative integrals, $N(r)$. T = 250 K (open circles, solid line); T = 384 K (open squares, dashed line). Middle (top) panels: two-dimensional, position-orientation distribution functions at high (low) temperatures. The color code identifies isolevels according to the normalized right-hand-side scale.

Our analysis of intermolecular density fluctuations will be based on the consideration of two-dimensional, site−site pair correlation functions of the following type:

$$g_{\alpha\gamma}(r) = \frac{1}{2\pi r \rho_s N_{\mathrm{Im}}} \sum_i \sum_{j\neq i} \langle \delta(|\mathbf{r}_i^{\alpha} - \mathbf{r}_j^{\gamma}| - r)\rangle \qquad (3)$$

where $\mathbf{r}_i^{\alpha}$ denotes the coordinate of site α in the ith molecule ($1 \leq i \leq N_{\mathrm{Im}}$) and $\langle ... \rangle$ denotes an equilibrium ensemble average. Given the structural characteristics already observed in the bulk,[31] one can anticipate that the relevant correlations will be those involving the three sites participating in HB, i.e., H2, N1, and N2. Results for the monolayer appear in the bottom panel of Figure 3. The most prominent peak corresponds to the H2−N2 pair (open circles) and is located at $r \sim 2$ Å. Although a direct comparison between the 2d monolayer and 3d results is not totally rigorous, we remark that the magnitude of this peak in the former system is clearly larger and its position is slightly shifted toward smaller distances, compared to the location observed in the liquid (dashed line). The changes are even more marked in the case of the intermolecular N1−N2 spatial correlations where, in addition to the shift toward smaller

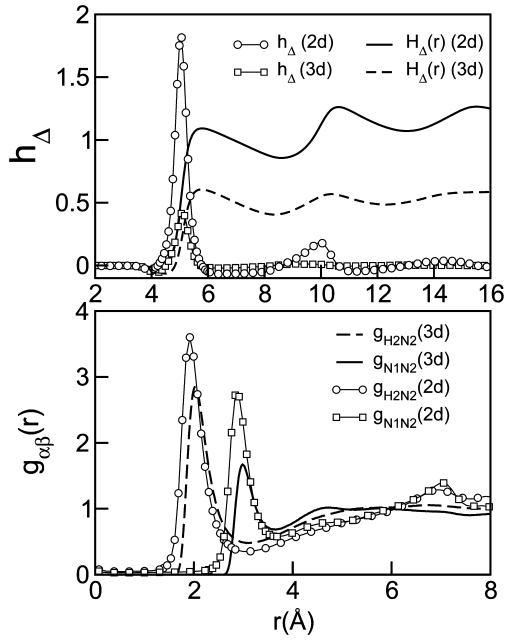

Figure 3. Bottom panel: site−site pair correlation functions for a 2d adsorbed Im monolayer at T = 384 K. Also shown are results for the isotropic bulk liquid at the same temperature. Top panel: Results for $h_{\Delta}(r)$ for the 2d adsorbed Im monolayer (open circles) and for the isotropic bulk liquid (open squares). The solid and dashed lines correspond to cumulative integrals $H_{\Delta}(r)$ (see text).

distances of the peak located at r = 3.1 Å, one observes a much more marked, ∼ 60% increment of its magnitude (squares versus solid lines). The picture that emerges from these observations would suggest that the combined effects derived from the planar molecular geometry and the attractive interactions promoted by the underlying graphite sheet would lead to stronger hydrogen bonds and a more compact packing of the monolayer, compared to the scenario that would prevail in the isotropic liquid phase.

A more vivid picture of the latter observations can be obtained from the snapshot shown in Figure 4, where we present a typical configuration of the monolayer. For clarity purposes, only the three sites participating in HB are displayed. At a first glance, the overall structure can be cast in terms of a set of winding, strand-like domains that span along sizable fractions of the simulation box. An inspection of several trajectories also reveals that these structures persist along typical time intervals of a few tens of picoseconds before undergoing major modifications in their overall shape and exchange of their constituents. Still, for the temperature and system size examined, the magnitude of the orientational correlations remains insufficient to promote symmetry-breaking, nematic-like liquid-crystal structures which have been reported in other simulation studies dealing with adsorbed monolayers.[19]

Clearly, the previous description reveals an important enhancement of the local orientational correlations which can be gauged from more quantitative grounds by considering basic elements borrowed from the theory of classical dipolar fluids.[32] In particular, we found it instructive to analyze the following correlation function:

dx.doi.org/10.1021/jp508913w | J. Phys. Chem. B XXXX, XXX, XXX−XXX

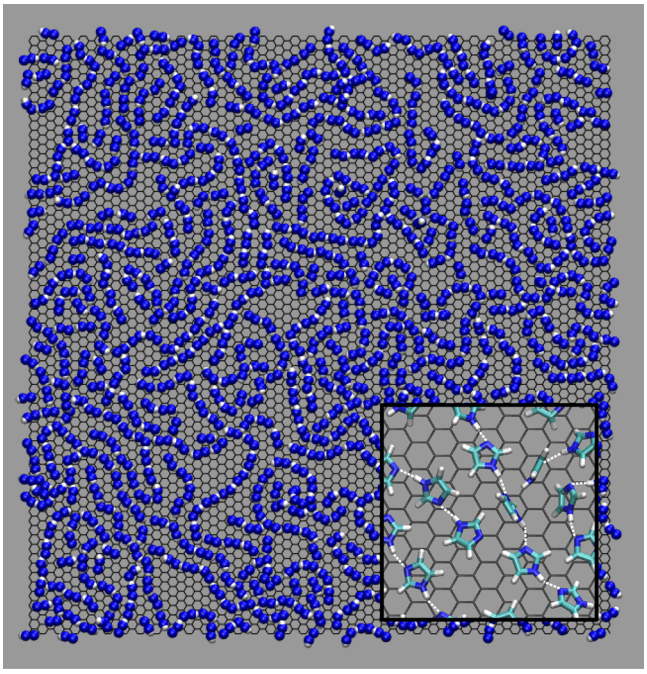

Figure 4. Snapshot of a typical configuration for an adsorbed layer at T = 384 K. Color code: N1 and N2 (blue); H2 (white) sites. The inset shows a zoomed picture of the local HB connectivity.

$$h_{\Delta}(r) = \frac{1}{2\pi r \rho_s N_{\mathrm{Im}}} \sum_i \sum_{j \neq i} \langle \delta(|\mathbf{R}_i - \mathbf{R}_j| - r)(\mathbf{r}_i^{\mathrm{NN}} \cdot \mathbf{r}_j^{\mathrm{NN}}) \rangle \tag{4}$$

where $\mathbf{R}_i$ represents the center of mass of the ith imidazole and $\hat{\mathbf{r}}_i^{\mathrm{NN}}$ represents a unit vector along the $\mathbf{r}_i^{\mathrm{N1}} - \mathbf{r}_i^{\mathrm{N2}}$ direction. In the top panel of Figure 3 we present results for $h_{\Delta}(r)$ and its cumulative integral; namely,

$$H_{\Delta}(r) = 2\pi\rho_s \int_0^r h_{\Delta}(r') r' \, \mathrm{d}r' \tag{5}$$

Note that the value of $H_{\Delta}(r)$ at large distances is determined by the degree of persistence of orientational correlations, as one moves away from a tagged Im molecule. Expressed in terms of the magnitude of $H_{\Delta}(r \sim 15$ Å), one can conclude that orientational correlations articulated via nearly colineal [N2···N1−H2]···[N2···N1−H2] segments of neighboring Im molecules are between 2 and 3 times stronger in the 2d film, compared to the ones registered in the bulk.

B. Dynamical Characteristics. We will turn to the analysis of time-dependent properties of the monolayer. From a dynamical perspective, the stronger characteristics of the intermolecular HB previously described are clearly manifested in orientational time correlation functions. In the bottom panel of Figure 5 we present results for

$$C_{\mathrm{NN}}(t) = \frac{1}{N_{\mathrm{Im}}} \sum_{i=1}^{N_{\mathrm{Im}}} \langle \hat{\mathbf{r}}_i^{\mathrm{NN}}(t) \cdot \hat{\mathbf{r}}_i^{\mathrm{NN}}(0) \rangle \tag{6}$$

In the film, the latter function provides information about the decorrelation of rotational motions around axes perpendicular to the molecular plane. After a short, sub-picosecond transient, the behavior of $C_{\mathrm{NN}}(t)$ can be reasonably well approximated by a single exponential, with characteristic time, τ_{NN}, of the order of ∼30 ps. The comparison between the 2d- and the 3d decays

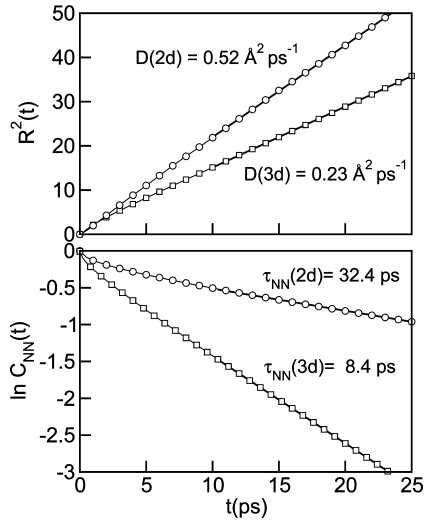

Figure 5. Bottom panel: orientational correlation function for an adsorbed Im monolayer at T = 384 K (circles). Also shown are results for the isotropic bulk liquid at the same temperature (squares). Top panel: mean square displacement for 2d and 3d systems. The thick solid lines represent linear regressions computed for t > 10 ps.

shows that the latter parameter presents a ∼4-fold increment, compared to the similar time scale observed in bulk Im.

The trends for the translational dynamics differs at a qualitative level. In the top panel of Figure 5, we present results for 2d and 3d mean square displacements; namely,

$$\mathcal{R}^2 = \frac{1}{N_{\mathrm{Im}}} \sum_{i=1}^{N_{\mathrm{Im}}} \langle |\mathbf{R}_i(t) - \mathbf{R}_i(0)|^2 \rangle \tag{7}$$

From the long-time lineal behavior, one can extract the corresponding diffusion coefficients, according to

$$D = \frac{1}{2d} \lim_{t \to \infty} \left(\frac{\mathcal{R}^2(t)}{t} \right) \tag{8}$$

Contrasting with the orientational dynamics, the reduction in the system dimensionality promotes an increment in the diffusion of the adsorbed layer by a factor of approximately ∼2 (see Figure 5). A comparative analysis of the nature of the relevant density fluctuations that may control particle transport in the liquid adlayer and the 3d isotropic liquid phase is not straightforward. Note that, in the 2d case, the net displacements are the results of a complex interplay between individual and collective modes, all of them modulated by the presence of two interfaces: (i) the underlying Im−graphite one and (ii) the upper, liquid−gas-like, free interface. We will not speculate furthermore in this aspect, although we remark that similar disparities between the diffusion coefficients in films and bulk environments have been reported in simulations of benzene monolayers adsorbed on graphite,[23,24] even though the structural characteristics of the latter film and the one analyzed here are clearly well differentiated.

Results from scattering experiments reported in ref 17 suggest that the diffusion of the 2d adsorbed fluid phase might be anisotropic, due to the presence of two nonequivalent directions along the graphite surface. Moreover, experimental signals were interpreted in terms of two diffusion coefficients: $D_1 \sim 0.81$ Å^2 ps^{-1} and a second one, D_2, which would be, at least, 1 order of magnitude smaller than D_1. Looking for

dx.doi.org/10.1021/jp508913w | J. Phys. Chem. B XXXX, XXX, XXX−XXX

additional simulation evidence to support this observation, we computed a series of 10 mean square 2d displacements, spanning all possible orientations with respect to the main symmetry axes of the substrate. In all cases, within the statistical errors of our simulation experiments, we failed to detect any anisotropy in the long-time behavior of the different $\mathcal{R}^2$. Yet, we did find differences in the short-time characteristics of the translational motions. Our analysis of this temporal regime was based on the decomposition of the full time correlation functions for the center of mass velocity,[33] $\mathbf{V}_i$; namely,

$$C_{vv}(t) = \frac{1}{N_{Im}} \sum_{i=1}^{N_{Im}} \langle \mathbf{V}_i(t) \cdot \mathbf{V}_i(0) \rangle \tag{9}$$

into parallel $C_{vv}^{\parallel}(t)$ and perpendicular $C_{vv}^{\perp}(t)$ contributions; namely,

$$C_{vv}^{\parallel}(t) = \frac{1}{N_{Im}} \sum_{i=1}^{N_{Im}} \langle \mathbf{V}_i^{\parallel}(t) \cdot \mathbf{V}_i^{\parallel}(0) \rangle$$

$$C_{vv}^{\perp}(t) = \frac{1}{N_{Im}} \sum_{i=1}^{N_{Im}} \langle \mathbf{V}_i^{\perp}(t) \cdot \mathbf{V}_i^{\perp}(0) \rangle \tag{10}$$

where $\mathbf{V}_i^{\parallel}(t) = [\mathbf{V}_i(t) \cdot \hat{\mathbf{r}}_{NN}(0)]\hat{\mathbf{r}}_{NN}(0)$ and $\mathbf{V}_i^{\perp}(t) = \mathbf{V}_i(t) - \mathbf{V}_i^{\parallel}(t)$. Results for the three velocity autocorrelation functions and their corresponding cosine Fourier transforms are shown in the top and bottom panels of Figure 6, respectively. The decay of $C_{vv}(t)$ is characterized by a couple of sub-picosecond, underdamped oscillations at ~200 and ~450 fs, before dying off beyond 1 ps. The decomposition of C_{vv} into parallel and perpendicular directions reveals that the latter oscillations arise mainly from parallel modes whereas the decay of $C_{vv}^{\perp}(t)$ looks practically structureless and somewhat slower. The analysis of the Fourier transforms provides more clear evidence of this feature: Note that beyond $\omega \gtrsim 120$ cm^{-1}, the characteristics of $\hat{C}_{vv}(\omega)$ are clearly dominated by those of $\hat{C}_{vv}^{\parallel}(\omega)$, whereas the main contributions to the low-frequency shoulder come mostly from perpendicular modes. The overall picture that emerges from this analysis suggests that the presence of the thread-like structures controlled by the strong H-bonds would lead to higher frequency dynamical modes, mostly along directions parallel to the local thread-like structure whereas perpendicular modes would dominate the low-frequencies branch of the $\hat{C}_{vv}(\omega)$. Moreover, one can make an equivalent interpretation in terms of the corresponding spatial displacements: in the inset of the top panel of Figure 6 we show results for the short-time behavior of the mean square displacements obtained by implementing a similar projection to the one operated in the center of mass velocities. Clearly, the parallel curve lies below the perpendicular one, indicating that high-frequency modes are less efficient in promoting net displacements of the adsorbed molecules. Of course parallel and perpendicular projections practically coincide with their common asymptotic, $0.5\,\mathcal{R}^2(t)$ limit for $t \gtrsim 10$ ps.

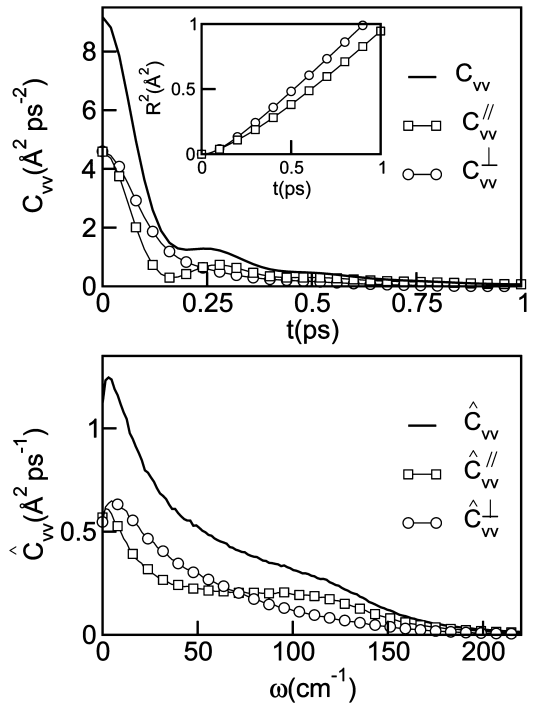

Figure 6. Top panel: Center of mass velocity autocorrelation function for the Im adlayer (solid line). Also shown are parallel (open squares) and perpendicular (open circles) contributions (see text). The inset shows the corresponding decompositions of the short-time behavior of the mean square displacements. Bottom panel: Fourier transforms of the different autocorrelation functions. Same labeling as the top panel.

IV. CONCLUDING REMARKS

In this work, we have presented molecular dynamics results that provide new insights about structural and dynamical characteristics of saturated, liquid-like monolayers of Im, physisorbed onto a planar graphite substrate. Our simulations predict that, upon adsorption, Im molecules can adopt two different orientations with respect to the plane of the underlying substrate with similar probabilities. Those lying closer to the solid phase respond to the attraction from the plane substrate by orienting their molecular planes parallel to the substrate whereas those located in farthermost positions exhibit slanted orientations. When compared to results from 3d isotropic phases, the 2d spatial correlations between sites participating in hydrogen bonding reveal global shortenings of donor−acceptor N1−N2 and H2−N2 distances and much more marked fluctuations. As a result, the prevailing 2d packing can be cast in terms of mesoscopic domains composed by, typically, tens of molecules in a winding, chain-like arrangement articulated by hydrogen bonds. At the thermodynamic conditions investigated, the magnitude of these orientational correlations—induced by the combined effects from intermolecular HB and the constraints imposed by the attractions with the substrate—was found to be insufficient to promote symmetry-breaking in the orientational structure of the adlayer over macroscopic length scales.

From the dynamical side, the stronger nature of the intramolecular interactions leads to a sensible, 4-fold increment in the characteristic time scales describing rotational motions, compared to the corresponding 3d scenario. More interestingly, the presence of a more ordered structure described in terms of the prevailing orientational distributions benefits translational displacements. Although a deeper analysis is surely called for, at this point we can speculate that the increment observed in the corresponding 2d diffusion coefficient could be the result of the presence of collective dynamical modes which are absent in more "disordered", 3d bulk phases. Our simulations showed no signs of anisotropic diffusive characteristics along preferential directions dictated by the atomic arrangement of the substrate. This observation clashes with the physical interpretation of

dx.doi.org/10.1021/jp508913w | J. Phys. Chem. B XXXX, XXX, XXX−XXX

previous diffraction experiments[17] and requires further analysis. On the other hand, we did identify differences in the short-time dynamics along parallel and perpendicular directions with respect to the instantaneous N1−N2 direction, which is the relevant one involved in the orientational correlations within the surface domains. The parallel projected velocity autocorrelation function exhibits a faster decay, compared to its perpendicular counterpart, a fact which is consistent with shorter effective displacements along the former direction. Yet, within the uncertainties of our simulations, the long-time characteristics of the corresponding mean square displacements look identical. We are confident that the previous observations will provide a physically meaningful benchmark for the correct interpretation of results from simulation experiments of proton transfer in Im films, which we are currently undertaking.

AUTHOR INFORMATION

Corresponding Author

*E-mail: dhlaria@cnea.gov.ar.

Notes

The authors declare no competing financial interest.

ACKNOWLEDGMENTS

J.R., M.D.E., and D.L. are staff members of CONICET (Argentina).

REFERENCES

(1) *Electron and Proton Transfer in Chemistry and Biology*; Muller, A., Ratajczak, H., Junge, W., Diemann, E., Eds.; Elsevier: New York, 1992.

(2) Jeffrey, G. A.; Junge, W.; Diemann, E. *Hydrogen Bonding in Biological Structures*; Springer: Berlin, 1994.

(3) Marx, D.; Tuckerman, M. E.; Hutter, J.; Parrinello, M. The Nature of the Hydrated Excess Proton in Water. *Nature* **1999**, *397*, 601−604.

(4) Vuilleumier, R.; Borgis, D. Quantum Dynamics of an Excess Proton in Water using an Extended Empirical Valence-bond Hamiltonian. *J. Phys. Chem. B* **1998**, *201*, 4261−4264.

(5) Knight, C.; Voth, G. A. The Curious Case of the Hydrated Proton. *Acc. Chem. Res.* **2012**, *45*, 101−109.

(6) von Grotthus, C. J. T. Mémoire sur la Décomposition de l'Eau et des Corps qu'elle tient en Dissolution a l'Aide de l'Éléctricité Galvanique. *Ann. Chim.* **1806**, *LVIII*, 54−73.

(7) Chen, H.; Yan, T.; Voth, G. A. A Computer Simulation Model for Proton Transport in Liquid Imidazole. *J. Phys. Chem. A* **2009**, *113*, 4507−4517.

(8) Daycock, J. T.; Jones, G. P.; Evans, J. R. N.; Thomas, J. M. Rotation of Imidazole in the Solid State and Its Significance in Deciding the Nature of Charge Migration in Biological Materials. *Nature* **1968**, *218*, 672−673.

(9) Münch, W.; Kreuer, K.-D.; Silvestri, W.; Maier, J.; Seifert, G. The Diffusion Mechanism of an Excess Proton in Imidazole Molecule Chains: First Results of an Ab Initio Molecular Dynamics Study. *Solid State Ionics* **2001**, *110*, 437−443.

(10) Li, A.; Cao, Z.; Li, Y.; Yan, T.; Shen, P. Structure and Dynamics of Proton Transfer in Liquid Imidazole. A Molecular Dynamics Simulation. *J. Phys. Chem. B* **2012**, *116*, 12793−12800.

(11) Tölle, P.; Calvacanti, W. L.; Hoffman, M.; Köhler, C.; Frauenheim, T. Modelling of Proton Diffusion in Immobilised Imidazole Systems for Application in Fuel Cells. *Fuel Cells* **2008**, *8*, 236−243.

(12) Kreuer, K.-D.; Paddison, S. J.; Spohr, E.; Schuster, M. Transport in Proton Conductors for Fuel-Cell Applications: Simulations, Elementary Reactions, and Phenomenology. *Chem. Rev.* **2004**, *104*, 4637−4678.

(13) Kreuer, K.-D.; Fuchs, A.; Ise, M.; Spaeth, M.; Maier, J. Imidazole and Pyrazole-Bases Proton Conducting Polymers and Liquids. *Electrochim. Acta* **1998**, *43*, 1281−1288.

(14) Harvey, J. A.; Basak, D.; Venkataraman, D.; Auerback, S. M. Simulating Hydrogen-Bond Clustering and Phase Behavior of Imidazole Oligomers. *Mol. Phys.* **2012**, *110*, 957−966.

(15) Tölle, P.; Köhler, C.; Marschall, R.; Sharigi, M.; Wark, M.; Frauenheim, T. Proton Transport in Functionalised Additives for PEM Fuel Cells: Contributions from Atomistic Simulations. *Chem. Soc. Rev.* **2012**, *42*, 5143−5159.

(16) Cavalcanti, W. L.; Portaluppi, D. F.; Joswig, J.-O. Preconditioning Immobilized Imidazole Arrays for Optimal Proton-Transfer Feasibility. *J. Chem. Phys.* **2010**, *133*, No. 104703.

(17) Monkenbusch, M.; Lauter, H. J. Structure and Dynamics of a 2d Hydrogen Bonded Adlayer-Imidazole on Grafoil. *Surf. Sci.* **1987**, *191*, 547−578.

(18) Feng, H.; Becker, K. E.; Zhou, J.; Fichthorn, K. A. Molecular Thin Films on Solid Surfaces: Mechanisms of Melting. *Langmuir* **2012**, *28*, 7382−7392.

(19) Watanabe, G.; Saito, J.-i.; Fujita, Y.; Tabe, Y. Molecular Dynamics Simulation Study of Two-Dimensional Diffusion Behavior in Smectic Liquid Crystalline Monolayers. *J. Phys. Soc. Jpn.* **2013**, *82*, No. 084603.

(20) Firlej, L.; Kutcha, B.; Roth, M. W.; Connolly, M. J.; Wexler, C. Structural and Phase Properties of Tetracosane Monolayers Adsorbed on Graphite: An Explicit Hydrogen Molecular Dynamics Study. *Langmuir* **2008**, *24*, 12392−12397.

(21) Diama, A.; Matthies, B.; Herwig, K. W.; Hansen, F. Y.; Criswell, L.; Mo, H.; Bai, M.; Taub, H. Structure and Phase transitions of Monolayers on Intermediate Length n-Alkanes on Graphite Studied by Neutron Diffraction and Molecular Dynamics Simulation. *J. Chem. Phys.* **2009**, *131*, No. 084707.

(22) Wexler, C.; Firlej, L.; Kuchta, B.; Roth, M. W. Melting of Hexane Monolayers Adsorbed on Graphite: The Role of Domains and Defect Formation. *Langmuir* **2009**, *25*, 6596−6598.

(23) Matties, M. A.; Hentschke, R. Molecular Dynamics Simulation of Benzene on Graphite. 1. Phase Behavior of Adsorbed multilayers. *Langmuir* **1996**, *12*, 2495−2500.

(24) Matties, M. A.; Hentschke, R. Molecular Dynamics Simulation of Benzene on Graphite. 2. Phase Behavior of Adsorbed Multilayers. *Langmuir* **1996**, *12*, 2501−2504.

(25) Fouquet, P.; Johnson, M. R.; Hedgeland, H.; Jardine, A. P.; Ellis, J.; Allison, W. Molecular Dynamics Simulations of the Diffusion of Benzene Sub-monolayers Films on Graphite Basal Plane Surfaces. *Carbon* **2009**, *47*, 2627−2639.

(26) MacKerell, J. A. D.; Banavali, N.; Foloppe, N. Development and Current Status of the CHARMM Force Field for Nucleic Acids. *Biopolymers* **2001**, *56*, 257−265.

(27) Darden, T. A.; York, D. M.; Pedersen, L. G. Particle Mesh Ewald: An N log(N) Method for Ewald Sums in Large Systems. *J. Chem. Phys.* **1993**, *98*, 10089−10092.

(28) Essmann, U.; Perera, L.; Berkowitz, M. L.; Darden, T.; Lee, H.; Pedersen, L. G. A Smooth Particle Mesh Ewald Method. *J. Chem. Phys.* **1995**, *103*, 8577−8593.

(29) Larese, J. Z.; Passell, L.; Heidemann, A. D.; Richter, D.; Wicksted, J. P. Melting in Two Dimensions: The Ethylene-on-Graphite System. *Phys. Rev. Lett.* **1988**, *61*, 432−435.

(30) Möller, M. A.; Klein, M. L. The Continuous Melting Transition of Ethylene on Graphite: A Molecular Dynamics Study. *Chem. Phys. Lett.* **1989**, *129*, 235−239.

(31) Shaik, M. S.; Liem, S. Y.; Yuan, Y.; Popelier, P. L. A. Simulation of Liquid Imidazole Using a High-Rank Quantum Topological Electrostatic Potential. *Phys. Chem. Chem. Phys.* **2010**, *12*, 15040−15055.

(32) Hansen, J.-P.; McDonald, I. R. *Theory of Simple Liquids*; Academic Press: London, 2006; Chapter 11.

(33) Barojas, J.; Levesque, D.; Quentrec, B. Simulation of Diatomic Homonuclear Liquids. *Phys. Rev. A* **1973**, *7*, 1092−1104.